Computers & Geosciences 58 (2013) 54–61

Contents lists available at SciVerse ScienceDirect

Computers & Geosciences

journal homepage: www.elsevier.com/locate/cageo

A wetting and drying scheme for ROMS

John C. Warner [a,*], Zafer Defne [a,b], Kevin Haas [b], Hernan G. Arango [c]

[a] U.S. Geological Survey, Coastal and Marine Geology Program, 384 Woods Hole Rd, Woods Hole, MA 02543, USA
[b] Georgia Institute of Technology, 210 Technology Circle, Savannah, GA 31407, USA
[c] Institute for Marine and Coastal Sciences, Rutgers—The State University of New Jersey, New Brunswick, NJ 08901, USA

ARTICLE INFO

Article history:
Received 25 January 2013
Received in revised form
8 May 2013
Accepted 16 May 2013
Available online 24 May 2013

Keywords:
Wetting and drying
ROMS
Cell-face blocking

ABSTRACT

The processes of wetting and drying have many important physical and biological impacts on shallow water systems. Inundation and dewatering effects on coastal mud flats and beaches occur on various time scales ranging from storm surge, periodic rise and fall of the tide, to infragravity wave motions. To correctly simulate these physical processes with a numerical model requires the capability of the computational cells to become inundated and dewatered. In this paper, we describe a method for wetting and drying based on an approach consistent with a cell-face blocking algorithm. The method allows water to always flow into any cell, but prevents outflow from a cell when the total depth in that cell is less than a user defined critical value. We describe the method, the implementation into the three-dimensional Regional Oceanographic Modeling System (ROMS), and exhibit the new capability under three scenarios: an analytical expression for shallow water flows, a dam break test case, and a realistic application to part of a wetland area along the Georgia Coast, USA.

Published by Elsevier Ltd.

1. Introduction

The wetting and drying process is a common occurrence in shallow water and coastal environments. This process can occur due to inundation on periodic time scales such as on the order of several days for storm surge, hours for the rise and fall of the tide, and minutes to seconds for infragravity wave motions on the shoreface. Wetting and drying is important for such physical processes as the development of shallow water nonlinear overtides (Aubrey and Speer, 1985; Parker, 1991; Blanton et al., 2002), can affect sediment transport in tidal channels and on tidal mud flats (Dronkers, 1986; Ralston and Stacey, 2007), and can be significant for biological processes that occur, for example, during the dry phase on a tidal mud flat algal mats (Gunatilaka, 1975). The wetting and drying are also significant during extreme events such as the inundation of coastal regions due to storm surge and wave driven run-up on beaches and dunes (Sallenger, 2000) that can cause extreme damage and coastal erosion.

To correctly simulate these processes in a numerical model requires the capability for cells to become 'dry' as the water level recedes and subsequent 'wetting' as the water level rises again. Incorporating these processes into numerical models has proven to be challenging over the years. There are many different formulations, each with specific caveats applicable to each specific model, with certain formulations that are more appropriate for specific model types. There exist many references in the literature that describe and summarize wetting and drying schemes for coastal ocean models, such as Ji et al. (2001), Oey (2005), and Casulli (2009), and their references within. For implicit type models, the incorporation of the wetting and drying can be implemented by removing dry cells from the matrix solution method. Recently Casulli (2009) describes a new semi-implicit formulation for allowing wetting and drying processes in an unstructured grid that does not require a minimum depth threshold.

For explicit type models, typically all of the computational cells are included in all the numerical computations during each time step. Therefore the capability to remove cells for certain steps is not an option and other techniques have been developed. The main difficulty faced is that the total depth in the computational cells cannot become identically zero because the numerical solution can involve division by the total cell depth. One approach is to modify the friction term and/or provide a leading coefficient that modifies the left-hand-side of the momentum equations, such that increased flow resistance occurs as the total water depth decreases. At some limit of shallowness, the flow will be in balance between the pressure gradient and bottom stress in regions that are deemed dry (Heniche et al., 2000; Burchard et al., 2004). This approach has advantages that tend to promote stability in the model and provide a smooth transition as the water levels decrease and subsequently increase. However, a disadvantage is

* Corresponding author. Tel.: +1 508 457 2237.
E-mail addresses: jcwarner@usgs.gov (J.C. Warner), zdefne@usgs.gov (Z. Defne), khaas@gatech.edu (K. Haas), arango@marine.rutgers.edu (H.G. Arango).

0098-3004/$ - see front matter Published by Elsevier Ltd.
http://dx.doi.org/10.1016/j.cageo.2013.05.004

that the increased resistance may create a delay in the timing of the incoming tide. Other approaches actually allow water depths to be positive or negative and the negative regions identify the locations that are considered dry. In these regions the friction coefficient varies with a functional dependence on the magnitude of the local total water depth. The approach can prevent a noisy pattern of transport between cells being switched on-and-off. Many other models have implemented variants of these formulations (Hamrick, 1994; Stelling and Duinmeijer, 2003; Chen et al., 2006).

The Princeton Ocean Model was modified to include wetting and drying (Oey, 2005, 2006). The method took advantage of the grid configuration for that model (Arakawa C grid) that has the cell fluxes at the interface. That implementation used a cell face blocking approach based on a criteria that if the depth of water at a cell face is below a user-defined threshold value, then the flux of water across that face is prevented. The formulation we employ is similar, however, our approach compares the total depth of water at the cell center where the water level is actually computed, not at the faces, to a user-defined threshold value. If the total depth is below the threshold value, then water flux is prevented from leaving that cell from all of its faces.

2. Methodology

The numerical ocean circulation model we use is the Regional Ocean Modeling System (ROMS), a three-dimensional, free surface, topography following numerical model, which solves finite difference approximations of Reynolds Averaged Navier Stokes (RANS) equations using hydrostatic and Boussinesq approximation with a split explicit time stepping algorithm (Shchepetkin and McWilliams, 2005, 2009a,b; Haidvogel et al., 2008). As described by Shchepetkin and McWilliams (2009a,b), currently there are four variations of ROMS-family codes. In this contribution we use a version based on the Rutgers University ROMS which was first introduced by Haidvogel et al. (2000). The model is solved on a horizontal Arakawa "C" grid. This grid configuration places the east u-component of velocity at the cell left and right faces (u-points), places the north v-component of the velocity at the cell front and back faces (v-points), and places values of most other prognostic variables (depth, water level, salinity, temperature, etc.) at the cell center (ρ-points).

As part of the original development, the ROMS model did not account for the processes of wetting and drying and thus limited the applicability of the model to exclude many shallow water coastal settings. In this context, we implemented a new method for wetting and drying into the ROMS model that will now allow applications of the model to shallow water environments. The methodology for wetting and drying developed and implemented into ROMS is a simple approach, however, the actual implementation was difficult due to the predictor–corrector time stepping algorithm for the depth-integrated momentum equations (described in detail by Shchepetkin and McWilliams, 2009a,b). The approach begins with a spatially-constant user defined minimum depth (D_{crit}). The value of D_{crit} is typically on the order of a few centimeters for estuarine or shoreline applications, but is a user-defined quantity and can be as small as a few millimeters (for idealized or laboratory tests) or as large as several meters. The specific value depends on the user defined application.

The numerical model is solved with an intricate split-explicit mode-splitting kernel. The majority of the wetting and drying methodology is implemented within the barotropic component of the mode splitting formulation. At each time step of the barotropic engine the total depth of water (D) at the cell center ρ-points is computed as the sum of the local bathymetry (h) and free surface displacement (η; $D=h+\eta$). The total depth is compared to the value of D_{crit}. If the total depth of water is less than D_{crit}, then the cell is considered 'dry' and no flux of water is permitted out of that cell for that barotropic time step. There are no other constraints imposed.

Our method has advantages over other methods in that it always allows water to flow into any dry cell at any time, allowing any cell that was previously dry to become wet. This approach does not limit arrival of the incoming tide. Additionally, our approach only prevents transport out of a cell if the total depth in that cell is less than D_{crit}. Other methods use the average water level at the u- or v- points to determine if water is allowed to drain out of an elevated region. If transport relied on the average depth at the cell face, then the average depth could be below D_{crit}, preventing flow out of cells and creating isolated wet patches. We anticipate that our approach may also produce isolated wet patches, however, they would most likely be due to local topography low points rather than the method. Even though our approach is simple, there are several caveats encountered to actually implement the method, as addressed below.

2.1. Land/sea masking

In order to resolve coastal topography, structured grid models use the approach of land/sea masking arrays. These arrays contain numerical values of 0 or 1 and are used during the computations to multiply prognostic values. Land points are locations that are not hydrodynamically active, will never have transport or water volume, and have a *land/sea mask*=0. Sea points evolve in time, and have a *land/sea mask*=1. For wetting and drying, we added an additional *wet/dry mask* that is spatially varying and evolves in time to allow regions to be wet (1) or dry (0). The *land/sea mask* and *wet/dry mask* are separate entities. A region with a *land/sea mask* of 0 will never contain water and therefore the *wet/dry mask* is set to 0 at these locations (Fig. 1, upper left land area). A region with *land/sea mask* of 1 can take both values of the *wet/dry mask*. If the *land/sea mask* is set to 1 as, for example, in an inter-tidal area (Fig. 1, center dark brown area), as the tide comes in and out the *wet/dry mask* can change values from dry (0) to wet (1). Regions further offshore (Fig. 1, blue area) with a *land/sea mask* of 1 that are deep (relative to D_{crit}) will typically remain wet and covered with water and will maintain a *wet/dry mask* value of 1. The *land/sea mask* is set by the user and never changes during the computation. The *wet/dry mask* is computed internally and is evaluated at every barotropic time step.

2.2. Barotropic momentum

The wet/dry methodology does not solve a prognostic equation. Instead it utilizes an approach that is engineered to work within the framework and methodology of this specific model. The basic aspect of the wet/dry algorithm is to compare the local value of total water depth in each cell to the user-defined critical value. If $D < D_{crit}$, then the cell is considered to be dry and the method only prevents outward transport of volume flux from that cell. Outward transport is inhibited by forcing the magnitudes of the depth-integrated momentum terms (*ubar* and *vbar*) to be zero. Inward flux is always permitted. These computations are performed during each barotropic time step.

The model uses an explicit predictor–corrector time stepping algorithm that has some advantages but also poses some complication to the actual wet/dry implementation. The *wet/dry mask* is actually characterized with three different masks, one for each of the *rho*, *u*, and *v* points. At the beginning of the barotropic time step, the *wet/dry mask* at each *rho* point (*rmask_wet*) is computed based on the value of the water level from the previous time step.

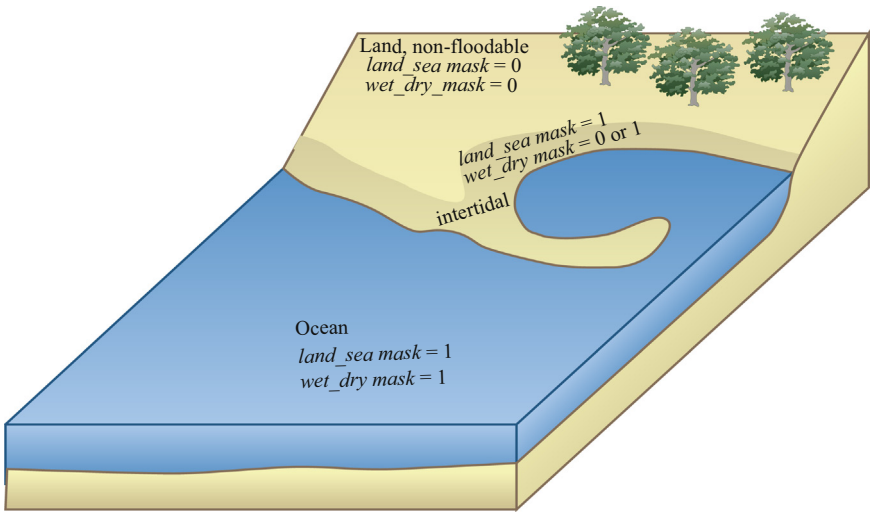

Fig. 1. Two types of grid masking: *land_sea* and *wet_dry*. The *land_sea mask* remains fixed for the entire simulation and identifies regions that will be permanently dry (*land_sea mask*=0, non-floodable) and regions that can be wet or dry (*land_sea mask*=1, floodable). The *wet_dry mask* varies during the simulation and identifies if a region is wet (*wet_dry mask*=1, $h+\eta > D_{crit}$) or dry (*wet_dry mask*=0, $h+\eta < D_{crit}$).

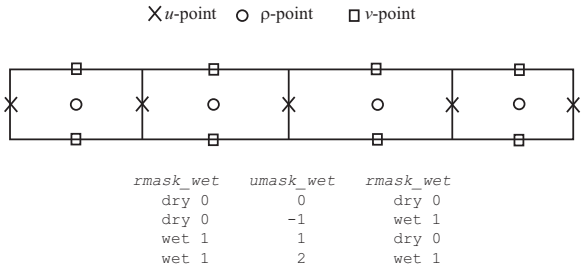

Fig. 2. Example section of simple grid identifying locations of ρ-, u-, and v- points. The *rmask_wet* identifies the wet/dry state at ρ-points and takes on values of 1 (wet) or 0 (dry). In the barotropic module, this relates to four different possibilities for the values of the *umask_wet* at u-points (similar for v-points).

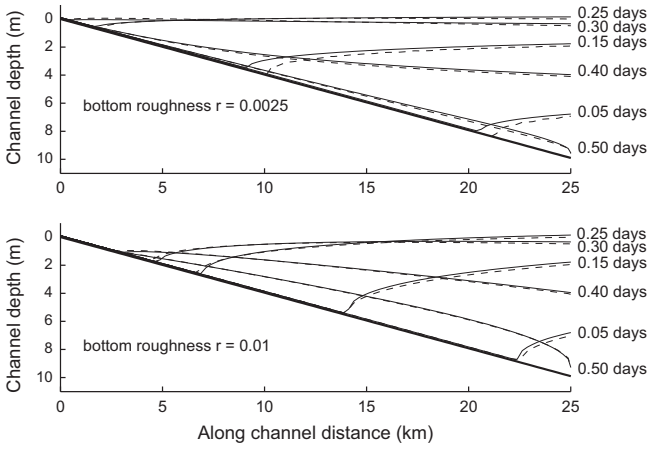

Fig. 3. Test case 1: Sloping channel. Thick solid line is the sloping channel bottom. Panels are for two different bottom roughness simulations of (A) $r=0.0025$ and (B) $r=0.01$. Results show free surface from Eq. 2 analytical solution (solid line) and model results (dashed line) for six instances in time (0.05, 0.15, 0.25, 0.30, 0.40, and 0.50 days).

Because the code uses an explicit time stepping scheme, the use of the previous time step does not create any inconsistencies for parallel programming. For each cell, if $D < D_{crit}$, then the cell is dry and the *rmask_wet* is set to 0, otherwise the *wet/dry mask* has a value of 1. The next step is to compute two more *wet/dry mask* arrays of *umask_wet* and *vmask_wet* at the u- and v- points. It was decided to use additional arrays for efficiency instead of adding conditional 'IF' statements that are computationally destructive.

During the barotropic time stepping, the *umask_wet* and *vmask_wet* arrays are first computed to identify the state of their adjacent cells. The *umask_wet* array (similar for v) can take on values of −1, 0, 1, or 2, based on the state of the *rmask_wet* on either side of the velocity point (Fig. 2). If the u-point is in between two cells that are both dry, the *umask_wet* will be 0. If both cells on either side of the u-point are wet, then *umask_wet* will have a value of 2. If one cell is wet and the other dry, *umask_wet* is set to have a value of −1 or 1 depending on which side is wet (−1 for wet on the right, and +1 for wet on the left). To enforce the wet/dry aspect, this value of the *umask_wet* (similar for v) is used to modify the value of the depth-averaged velocity ($ubar^{t+1}$) at the next time step as

$$ubar^{t+1} = ubar^{t+1} * \left(\begin{array}{l} 0.5 * umask\_wet * ||umask\,wet|-1|+ \\ (0.5 + umask\_wet * DSIGN(0.5, ubar^{t+1})) * (1-||umask\,wet|-1|) \end{array} \right) \quad (1)$$

The DSIGN is an intrinsic function that returns a value based on the magnitude of the first argument (0.5) and the sign of the second argument ($ubar^{t+1}$). The algorithm will modify the value of the new velocity accordingly. If the *umask_wet* is 0, then there should be no flow out of either cell and the $ubar^{t+1}$ is then computed to be zero from Eq. (1). If the *umask_wet* is 2, then both sides of the velocity point are wet and the flow is not affected by Eq. (1). If the value of *umask_wet* is −1, then Eq. (1) restricts the flow to only be in the negative x-direction (only allow flow to the left). If the flow was to the right, Eq. (1) will force this to become zero, enforcing the criteria that no flow is allowed out of a dry cell. If the *umask_wet* is 1, then Eq. (1) restricts the flow to only be in the positive x-direction, only allowing flow from a wet cell to a dry cell.

During the predictor/corrector algorithm, the computations of the barotropic velocities utilize values from previous time levels. During the wet/dry algorithm, these forcing terms are corrected to account for changes imposed to the momentum terms. After the barotropic time stepping, the *umask_wet* and *vmask_wet* arrays are set to 0 or 1 based on the average of all the barotropic steps during the wet_dry operations. These *umask_wet* and *vmask_wet* are then used in the computations during the baroclinic time stepping and for output purposes. It is important to note that the final values of *ubar* and *vbar* at the new time level are multiplied by this masking.

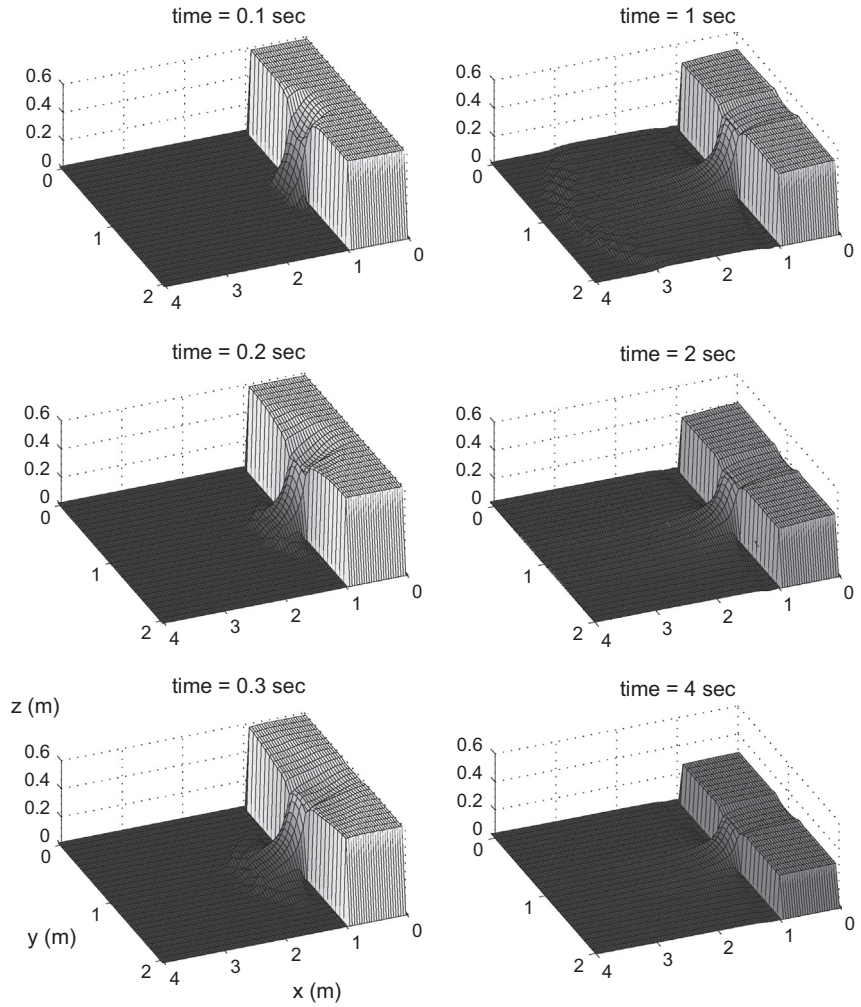

Fig. 4. Test Case 2: Dam break—plan views of free surface at different moments in time (0.1, 0.2, 0.3, 1.0, 2.0, and 4.0 s).

2.3. Baroclinic velocities

The baroclinic velocities are affected by being multiplied by the final wet_dry masking values. Therefore, at a cell face, there could have been an instance where volume flux occurred across that face during part of the barotropic time stepping, but the final values of both barotropic and baroclinic momentum would show zero transport. This is because the model does not output values on the barotropic (fast) time stepping, only the baroclinic time step. During initial testing of the algorithm, it was identified that instabilities occurred infrequently at times of rewetting. It was traced to the explicit imposition of the bottom stress during the predictor time stepping. This was avoided by imposing a limiter to prevent the bottom stress term from having a value large enough to change the sign of the velocity term.

3. Applications

We show the utility of the method with three applications: shallow water flow in a tidal channel; a dam break test case; and a realistic application along the US East Coast.

3.1. Tidal channel flow

This application was presented in Oey (2005) for flow in a one-dimensional tidal channel with a sloping bottom. Combining the depth averaged momentum and continuity equations, neglecting the convective acceleration terms, and using a linear bottom stress produces a non-linear advection-diffusion (Burger's type) equation (Eq. (7) in Oey 2005)

$$\frac{\partial D}{\partial t}+\left(\frac{2gDH_x}{r}\right)\frac{\partial D}{\partial x}=\frac{\partial}{\partial x}\left(\frac{gD^2}{r}\frac{\partial D}{\partial x}\right)-\frac{gD^2}{r}\frac{\partial^2 H}{\partial x^2} \tag{2}$$

where t is time, x is the along-channel distance, H_x is the bottom slope, g is gravitational acceleration, r is a linear bottom friction term.

Following Oey (2005), we applied our model to a simple test case of a 1-D sloping channel that ranges from $x=0$ at the landward end to $x=$L at the seaward boundary (Fig. 3). The channel length was set to be $L=25$ km, sloping with a relation of $H(x)=10x/L$. The depth was zero at closed landward boundary and increasing linearly to $D_0=10$ m at the open seaward. The channel was discretized into 100 cells in the along-channel direction resulting with a spacing of 250 m. The cross-channel spacing was performed with 5 cells at 200 m, but is laterally uniform and not significant. This was a depth-averaged simulation focused on the barotropic response of the wet–dry algorithm. The channel is initialized as dry with a D_{crit} of 0.10 m. The water level at the seaward end was oscillated sinusoidally with a period of 0.5 days as

$$\text{zeta\_east}=10.0\sin(\text{pi}/0.5t)-10.0 \tag{3}$$

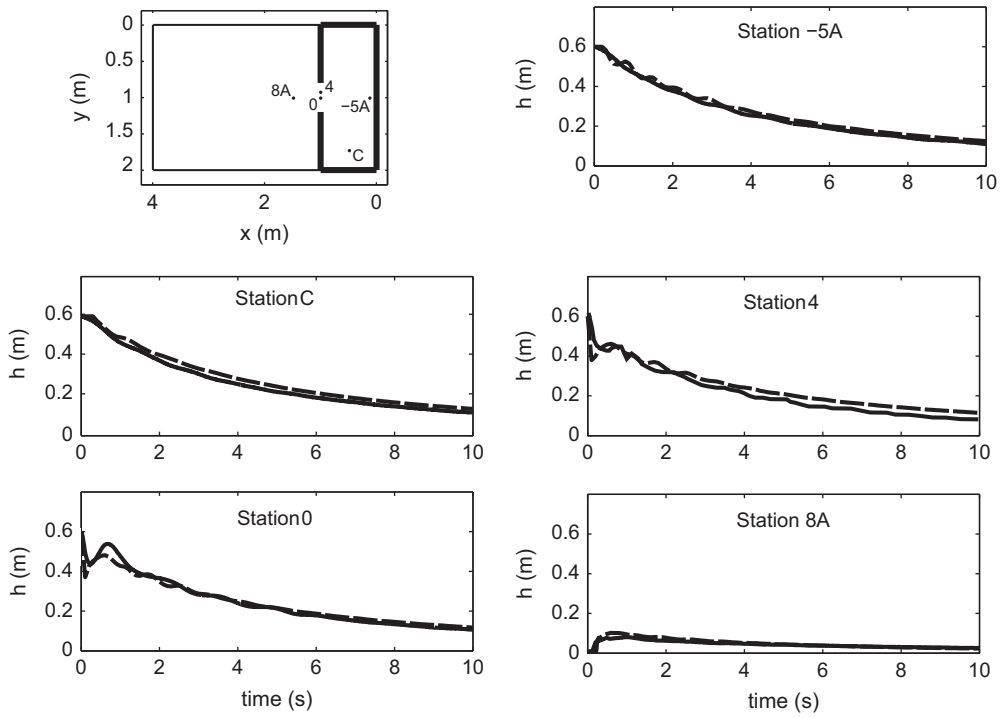

Fig. 5. Test Case 2: Dam break—time series plots from stations −5A, C, 4, 0, and 8A (shown in upper left panel) comparing measured water levels (solid line) and model results (dashed line).

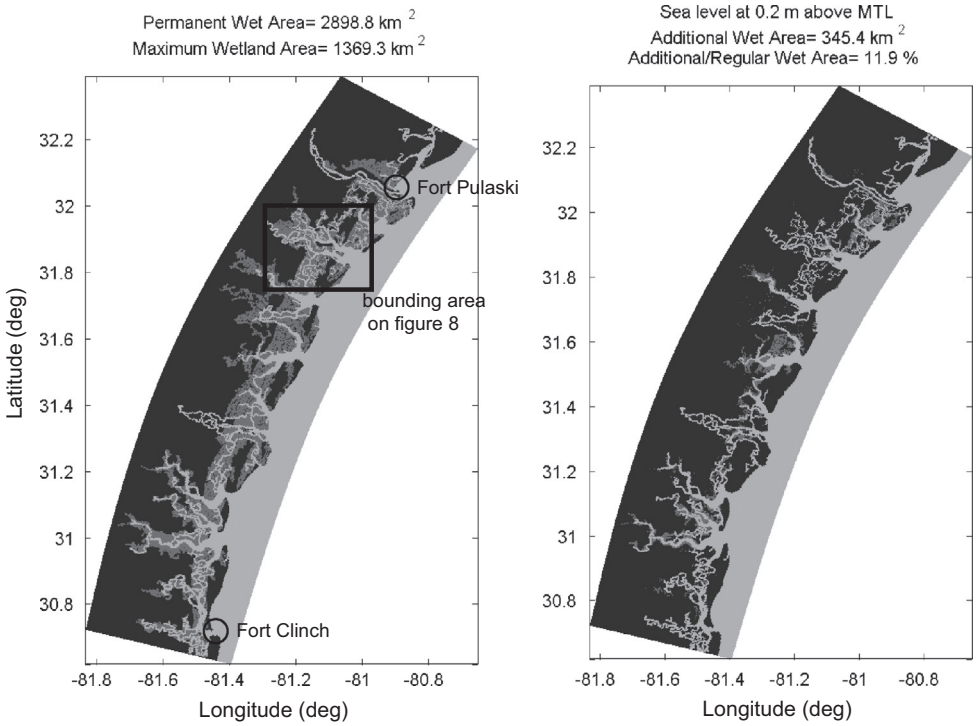

Fig. 6. Test case 3: Georgia wetlands. (a) Wetland area in the computational domain and (b) additional wet area for water level 0.2 m above MTL. Permanently dry cells (black), permanently wet cells (light gray), wetting drying cells (gray).

where t is time ranging from 0 to 0.5 days, with a 1 s time step. Two simulations were performed, both without the convective acceleration terms, and for different linear drag bottom roughness factors of $r=0.0025$ and $r=0.01$. Results of the free surface (Fig. 3) identify a strong agreement between the model and analytical solution (Eq. (2)), with average root mean square errors (RMSE) of 0.13 and 0.08 m for the two different roughness factors. The water levels are shown for six instances in time. A slight mis-agreement occurs at the leading edge of the advancing front for the case of weaker bottom friction during the wetting phase (for example, $r=0.0025$ top panel at time 0.05 and 0.15 days). For these instances the model is advancing the front slightly faster than the analytical approximation. Variations of D_{crit} did not affect the solution. Results are in agreement for the

stronger bottom friction and for all phases of the advancing and retreating water levels.

3.2. Dam break

This test consists of a basin of water that spills through an opening to flood an initially dry floodplain. Experimental measurements are available in the literature by Fraccarollo and Toro (1995), with a further investigation and comparison to different numerical simulations by Ferrari et al. (2010). The laboratory setup consisted of an enclosed basin measuring 1 m (x-direction) by 2 m (y-direction) (Fig. 4). The basin is initialized with a depth of 0.6 m. Centered on the edge of the basin is an opening measuring 0.40 m in the y-direction. At initialization the water in the basin is stationary but immediately begins to flow out the opening, flooding a flat floor. The flat floor extends 3 m in the x-direction, and has the same y-distance, and is initially dry. The flow is allowed to spill over the edges of the floor and exit the domain. The lab experiment was simulated numerically at the same spatial scales, discretized with 102 cells in the x-direction, 27 in the y-direction, resulting in grid spacings of 0.04 m and 0.08 m in the x- and y- directions, respectively. This simulation was performed in depth-averaged (shallow-water equations) mode to focus on the barotropic response, and was simulated using a time step of 0.0001 s for a total of 10 s. A three-dimensional simulation produces results similar to the depth-averaged simulation.

Fig. 4 shows results of the numerical simulations at six different instances in time of 0.1, 0.2, 0.3, 1.0, 2.0, and 4.0 s. The flow originates through the opening and immediately begins to spill across the floor. At first the flow spreads longitudinally more than laterally. Initially a rarefaction wave predicted by the model is in the tank above the outfall, but eventually moves outside the opening. The wave in the tank causes reflections and the simulation produces a wavy free surface in the basin. This behavior is consistent with shallow water equation approximations but not essentially consistent with the tank observations (Ferrari et al., 2010).

During the actual laboratory experiment, water levels were measured at many stations at a frequency of 0.01 s, and we chose to display results for five of them (−5A, C, 4, 0, and 8A; Fig. 5). Site −5A is located opposite the opening in the back of the basin. Site C is also in the basin and to the south of the opening. Sites 4 and 0 are in the opening and site 8A is on the floodplain. Time series of water level from the model (dashed lines) are compared to the observations (solid lines). In comparing the model and observations, the average RMSE is 0.02 m. In general, the model captures the timing of the flood pulse out of the basin and captures the steady draw down of the water level. The model appears to have more small scale oscillations of the water level than observed. Additional simulations of adding harmonic viscosity or increasing bottom friction were not attempted but could produce smoother results that would be more consistent with the measurements.

3.3. Georgia wetlands, USA

This application is based on a realistic setting along the US East Coast in Georgia. Results are included here to identify the applicability of the method to resolve a complicated realistic shallow estuarine wetland and tidal channel system. Numerical simulations were performed to determine tidal current stream power, for use as a potential source of renewable energy, as part of a separate effort described in full detail in Defne et al., (2011).

The numerical simulations were conducted along approximately 150 km of the Georgia coastline (Fig. 6a). The computational grid cell sizes ranged from 180 m inland to 330 m offshore. Approximately 47% of the grid is wetlands based on the National Wetlands Inventory (NWI) data. Although the maximum wetland area is achieved only at spring tides when the higher elevations are inundated, wetlands still accommodate significant amount of water in each tidal cycle. There is substantial additional wet area added by the wetlands once the water level rises above the Mean Tidal Level (MTL). For every 10 cm increase in the water level, about a hundred square kilometers additional area is inundated with sea water (Defne et al., 2011). The additional wet area 0.2 m above MTL is shown in Fig. 6b as an example. It was crucial to utilize the wetting and drying algorithm in ROMS in order to predict the hydrodynamics of such a system more accurately.

The model was run for a 32 days simulation. Time series for current magnitudes from Fort Pulaski near the Savannah River entrance and Fort Clinch at Cumberland Sound entrance demonstrate the amplification in the ebb currents when wetlands are incorporated in the model (Fig. 7). The additional volume of water in the tidal prism due to wetlands usually results in larger ebb and flood tide at the river mouths and bay entrances, while sometimes facilitating the modeling of tidal asymmetry due to stronger ebb flow.

An example for wetting and drying of the intertidal zone during a tidal cycle is shown in Fig. 8 for an area including the Ossabaw Sound on the southeast, Canooche River on the southwest and the Ogeechee River on the northwest. Shown in each panel is a plan view image that shows a snapshot of the distribution of wet and dry cells in the domain at every two hours, and a time series plot that displays the water level at the bay entrance for the same period. Panels a–b–c are for the flooding tide, and panels d–e–f are for the same area on the ebbing tide. The land elevation for the initially dry cells was calculated using 1 arc-second National Elevation Dataset from the U.S. Geological Survey Seamless Data Warehouse. Therefore, a unique flooding and dewatering pattern is observed as a result of the changing water level with respect to the real topography. The northeast part of the domain has the lowest elevation and closer to the bay entrance, therefore becomes inundated sooner (Fig. 8b) and stays wet longer (Fig. 8f). On the other hand, it takes longer for the

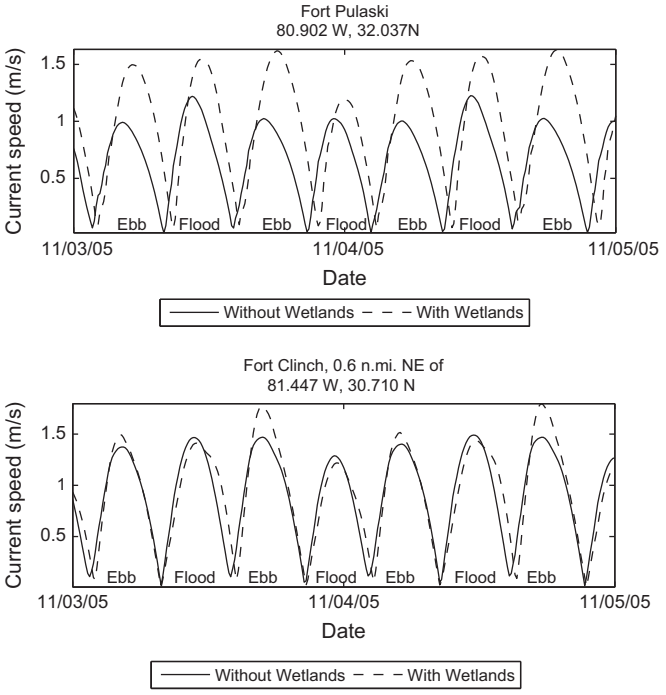

Fig. 7. Current magnitudes computed by the model with and without wetlands at (a) Fort Pulaski near Savannah River entrance and (b) Fort Clinch at Cumberland Sound entrance.

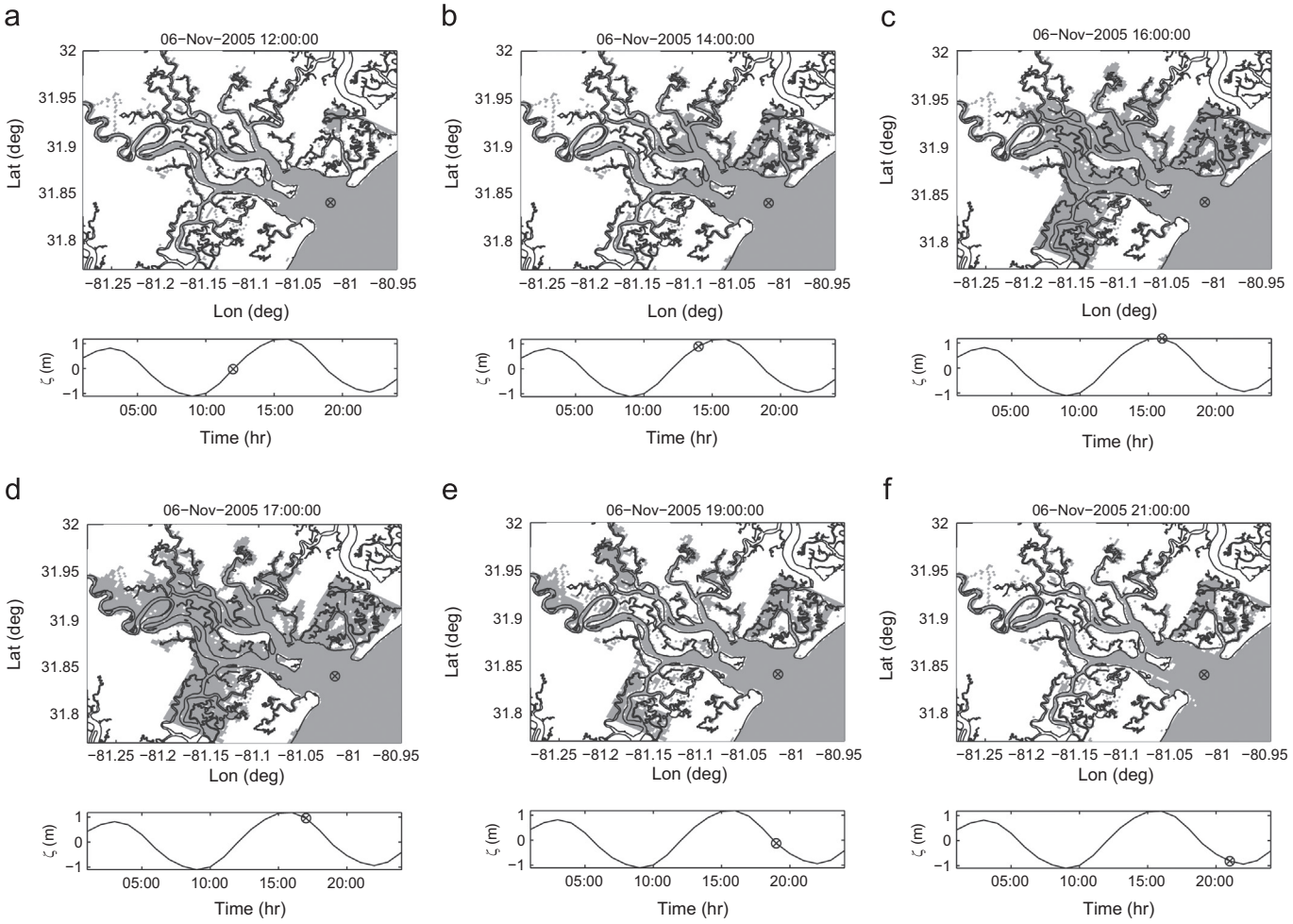

Fig. 8. The wetting and drying algorithm demonstrated on the Ossabaw Sound, GA during a flood (a–c) and ebb tide (d–f). Shaded regions indicate wet cells. Bottom panels display the water level time series from the bay entrance (as marked on each panel).

slightly higher land on the southwest and west to become inundated (Fig. 8c and d).

The benefit of the wetting and drying algorithm allows the wetlands to be included in the model and this provides a more realistic simulation that can capture the asymmetry between the ebb and flood currents. The tidal prism is not confined to the solid boundaries but varies according to the topography of the wetlands. The increased number of wet cells and the change in the tidal prism are found to significantly increase the tidal current magnitudes. The results from the model runs with wetlands are closer to NOAA predictions in general. For the main tidal constituents, the error in water level predictions are less than 0.05 m for amplitude and less than 20 min in phase, and less than a 10% difference in tidal currents. These results agree better with the measurements than the model runs that do not account for wetlands (Defne, 2011).

4. Summary

A method for wetting and drying has been implemented into the three-dimensional ROMS model. The method is based on a cell-face blocking approach during the barotropic phase of the computations. At each time step the total water depth in each cell is compared to a user-defined critical value. If the total water depth is below that critical value then that cell is deemed dry. The method prevents flow out of cells that are deemed dry. The method is simple, but required some intricate design due to the predictor–corrector time stepping. The fact that the model used a mode splitting approach helped to isolate the barotropic engine and allowed for the approach to be implemented more easily.

The method was applied to three scenarios of a sloping channel test case, a dam break laboratory study, and a realistic application to a network of tidal channels. Results compared well to analytical solutions, laboratory data, and field data identifying that the method is robust and applicable to a wide range of flow situations.

Acknowledgments

We thank the reviewers for their comments, open access to the ROMS modeling system, and to the Integration and Application Network (ian.umces.edu/symbols), University of Maryland Center for Environmental Science, for the courtesy use of their symbols and diagrams. We thank Dr. Luigi Fraccarollo for access to the data so that we may show comparisons to our simulations. We acknowledge support for studies demonstrated in this manuscript that were supported by the National Science Foundation, Division of Industrial Innovation and Partnerships (IIP) under the 3470 Z. Defne et al./Renewable Energy 36 (2011) 3461e3471 Partnerships for Innovation Program Grant IIP- 0332613, and from the Strategic Energy Institute at Georgia Institute of Technology via a Creating Energy Options grant and the 104B Georgia Water Resources Institute Funding Program, and also by the Department of Energy,

Wind and Hydropower Technologies Program award number DE-FG36-08GO18174 and by the state of Georgia.

References

Aubrey, D.G., Speer, P.E., 1985. A study of non-linear tidal propagation in shallow inlet/estuarine systems, Part 1observations. Estuarine, Coastal and Shelf Science 21, 185–205.

Blanton, J.O., Lin, G., Elstona, S.A., 2002. Tidal current asymmetry in shallow estuaries and tidal creeks. Continental Shelf Research 22, 1731–1743.

Burchard, H., Bolding, K., Villarreal, M.R., 2004. Three-dimensional modelling of estuarine turbidity maxima in a tidal estuary. Ocean Dynamics 54, 250–265.

Casulli, V., 2009. A high-resolution wetting and drying algorithm for free-surface hydrodynamics. International Journal for Numerical Methods in Fluids 60 (4) 391–408, http://dx.doi.org/10.1002/fld.1896.

Chen, C., Beardsley, R.C., Cowles, G., 2006. An Unstructured Grid, Finite-Volume Coastal Ocean Model FVCOM User Manual. SMAST/UMASSD-06-0602.

Defne, Z., 2011. Multi-Criteria Assessment of Wave and Tidal Power Along the Atlantic Coast of the Southeastern USA. Georgia Institute of Technology, Savannah, GA, Ph.D. thesis.

Defne, Z., Haas, K.A., Fritz, H.M., 2011. Numerical modeling of tidal currents and the effects of power extraction on estuarine hydrodynamics along the Georgia coast, USA. Renewable Energy 36, 3461–3471.

Dronkers, J., 1986. Tidal asymmetry and estuarine morphology. Netherlands Journal of Sea Research 20, 117–131.

Ferrari, A., Fraccarollo, L., Dumbser, M., Toro, E.F., Armanini, A., 2010. Three-dimensional flow evolution after a dam break. Journal of Fluid Mechanics 663, 456–477.

Fraccarollo, L., Toro, E.F., 1995. Experimental and numerical assessment of the shallow water model for two-dimensional dam-break type problems. Journal of Hydraulic Research 33, 843–864.

Gunatilaka, A., 1975. Some aspects of the biology and sedimentology of laminated algalmats from mannar lagoon, Northwest Ceylon. Sedimentary Geology 14 (4), 275–300.

Haidvogel, D.B., Arango, H.G., Hedstrom, K., Beckmann, A., Malanotte-Rizzoli, P., Shchepetkin, A.F., 2000. Model evaluation experiments in the North Atlantic Basin: simulations in nonlinear terrain-following coordinates. Dynamics of Atmosphere and Oceans 17 (32), 239–281.

Haidvogel, D.B., Arango, H.G., Budgell, W.P., Cornuelle, B.D., Curchitser, E., Di Lorenzo, E., Fennel, K., Geyer, W.R., Hermann, A.J., Lanerolle, L., Levin, J., McWilliams, J.C., Miller, A.J., Moore, A.M., Powell, T.M., Shchepetkin, A.F., Sherwood, C.R., Signell, R.P., Warner, J.C., Wilkin, J., 2008. Regional ocean forecasting in terrain-following coordinates: model formulation and skill assessment. Journal of Computational Physics 227, 3595–3624.

Hamrick, J.M., 1994. Application of the EFDC, Environmental Fluid Dynamics Computer Code to SFWMD Water Conservation Area 2A. A Report to South Florida Water Management District. JMH-SFWMD-94-01. In: Hamrick, J.M. (Ed.), Consulting Engineer, Williamsburg, VA, p. 126.

Heniche, M., Secretan, Y., Boudreau, P., Leclerc, M., 2000. A two-dimensional finite element drying–wetting shallow water model for rivers and estuaries. Advances in Water Resources 23, 359–372.

Ji, Z.G., Morton, M.R., Hamrick, J.M., 2001. Wetting and drying simulation of estuarine processes. Estuarine, Coastal, and Shelf Science 53, 683–700.

Oey, L.Y., 2005. A wetting and drying scheme for POM. Ocean Modelling 9, 133–150.

Oey, L.Y., 2006. An OGCM with movable land-sea boundaries. Ocean Modelling 13, 179–195.

Parker, B.B., 1991. The relative importance of the various non-linear mechanisms in a wide range of tidal interactions (review). In: Parker, B.B. (Ed.), Tidal Hydrodynamics, 1991. Wiley, New York, USA, pp. 237–268.

Ralston, D., Stacey, M.T., 2007. Tidal and meteorological forcing of sediment transport in tributary mudflat channels. Continental Shelf Research 27 (10–11), 1510–1527.

Sallenger, A.H., 2000. Storm impact scale for barrier islands. Continental Shelf Research 16 (3), 890–895.

Shchepetkin, A.F., McWilliams, J.C., 2005. The regional oceanic modeling system: a split-explicit, free-surface, topography—following coordinate oceanic model. Ocean Modeling 9 (4), 347–404, 〈http://dx.doi.org/10.1016/j.ocemod.2004.08.002〉.

Shchepetkin, A.F., McWilliams, J.C., 2009a. Correction and commentary for "Ocean forecasting in terrain—following coordinates: formulation and skill assessment of the regional ocean modeling system" by Haidvogel et al. Journal of Computational Physics 227, 3595–3624.

Shchepetkin, A.F., McWilliams, J.C., 2009b. Correction and commentary for "Ocean forecasting in terrain—following coordinates: formulation and skill assessment of the regional ocean modeling system" by Haidvogel et al. Journal of Computational Physics 228, 8985–9000.

Stelling, G.S., Duinmeijer, S.P.A., 2003. A staggered conservative scheme for every Froude number in rapidly varied shallow water flows. International Journal for Numerical Methods in Fluids 43, 1329–1354.